© 2022. Published by The Company of Biologists Ltd | Journal of Cell Science (2022) 135, jcs259344. doi:10.1242/jcs.259344

RESEARCH ARTICLE

Annexin A2 and Ahnak control cortical NuMA–dynein localization and mitotic spindle orientation

Aude Pascal, Emmanuel Gallaud, Regis Giet and Christelle Benaud*

ABSTRACT

Proper mitotic spindle orientation depends on the correct anchorage of astral microtubules to the cortex. It relies on the remodeling of the cell cortex, a process not fully understood. Annexin A2 (Anx2; also known as ANXA2) is a protein known to be involved in cortical domain remodeling. Here, we report that in HeLa cell early mitosis, Anx2 recruits the scaffold protein Ahnak at the cell cortex facing spindle poles, and the distribution of both proteins is controlled by cell adhesion. Depletion of either protein or impaired cortical Ahnak localization result in delayed anaphase onset and unstable spindle anchoring, which leads to altered spindle orientation. We find that Ahnak is present in a complex with dynein–dynactin. Furthermore, Ahnak and Anx2 are required for correct dynein and NuMA (also known as NUMA1) cortical localization and dynamics. We propose that the Ahnak–Anx2 complex influences the cortical organization of the astral microtubule-anchoring complex, and thereby mitotic spindle positioning in human cells.

This article has an associated First Person interview with the first author of the paper.

KEY WORDS: Annexin A2, Ahnak, Mitosis, Spindle orientation, Mitotic cortex

INTRODUCTION

Establishing a correct cell division axis, which depends on a precise positioning of the mitotic spindle, is crucial for the development of epithelial tissue and maintenance of its integrity. The orientation of cell division is specified at mitotic entry. As the mitotic spindle forms, it is positioned within the cell via its anchoring to the cell cortex. The robustness of this anchoring provides the mechanical force for the spindle to properly capture chromosomes, as well as dictating spindle orientation (di Pietro et al., 2016). Spindle orientation is a process controlled by both intrinsic and extrinsic cues (Kiyomitsu and Cheeseman, 2012; Théry et al., 2005). It is achieved through the interaction of spindle astral microtubules with the cortical-anchoring complex, composed of a highly evolutionarily conserved set of core proteins (di Pietro et al., 2016; Morin and Bellaïche, 2011). In prometaphase, the minus-end-binding motor protein dynein present at the tip of astral microtubules is recruited to the cortex through its association with cortical NuMA (also known as NUMA1) (Morin and Bellaïche, 2011). These anchoring elements localize at the cortex facing the spindle pole in a spatially constrained crescent shape. As prometaphase progresses, the oscillation of dynein from one side of the cortex to the opposite provides the pulling and pushing forces that are required for proper spindle positioning (Kiyomitsu and Cheeseman, 2012).

It is well established that the orientation of the mitotic spindle is affected by extrinsic signals such as cell adhesion and the positioning of neighboring cells (di Pietro et al., 2016). As cells enter and progress through mitosis, retractation fiber positioning drives the reorganization of the actin-based cell cortex and influences the localization of the spindle-anchoring complex within the cortex (Théry et al., 2005; van Leen et al., 2020; Machicoane et al., 2014). However, the precise molecular machinery that transduces extrinsic signals to precisely control spindle orientation is not yet fully understood.

Annexin A2 (Anx2; also known as ANXA2) is a member of the annexin family of small Ca^{2+}-binding proteins with high binding affinity for membrane phosphatidylinositols (PIPs). In interphase cells, Anx2 is preferentially enriched in cortical regions as part of a tetramer with the S100A10 protein (composed of two Anx2 subunits and two S100A10 subunits). Anx2 performs pleiotropic cellular functions, including the regulation of vesicular trafficking and the establishment of epithelial cell polarity (Grieve et al., 2012). Together with the giant (700 kDa) scaffold protein Ahnak, Anx2 drives the cortical cytoskeleton remodeling associated with the initial steps of epithelial cell polarization (Benaud et al., 2004). Consistent with its involvement in setting up specific submembranous cortical domains, Anx2 also participates in the organization of the cytokinetic ring in anaphase (Martin-Belmonte et al., 2007; Benaud and Prigent, 2016; Benaud et al., 2015). However, its role in other phases of mitosis had not yet been investigated.

We show here that the cortical Anx2–Ahnak complex is crucial for prometaphase progression and mitotic spindle orientation. Under the influence of cell adhesion, Anx2 regulates Ahnak localization at the cortex. Furthermore, impaired Ahnak localization there alters the constrained localization of the cortical NuMA–dynein complex. Altogether, our results show the essential contribution of the cortical Anx2–Ahnak complex in the establishment of spindle orientation.

RESULTS

Anx2 is required for prometaphase progression

To investigate the role of Anx2 in prometaphase progression, we generated two independent siRNAs that significantly decrease Anx2 expression levels in HeLa cells (Fig. 1A). Following cell synchronization at the G2/M transition by treatment with the CDK1 inhibitor RO-3306, we observed that Anx2 depletion hinders mitotic progression. Whereas the mitotic cells expressing Anx2 had progressed into anaphase 60 min after G2/M release, the Anx2-depleted cells had not yet reached anaphase onset (Fig. 1B). Time-lapse analysis further confirmed that Anx2 depletion significantly delayed anaphase entry (Fig. 1C). Whereas the control cells reached

Univ Rennes, CNRS, INSERM IGDR (Institut de Génétique et Développement de Rennes) - UMR 6290, ERL U1305, F-35000 Rennes, France.

*Author for correspondence (christelle.benaud@univ-rennes1.fr)

E.G., 0000-0002-7594-7309; R.G., 0000-0001-9027-5849; C.B., 0000-0001-9432-2331

Handling Editor: David Glover
Received 1 September 2021; Accepted 25 March 2022

Journal of Cell Science (2022) 135, jcs259344. doi:10.1242/jcs.259344

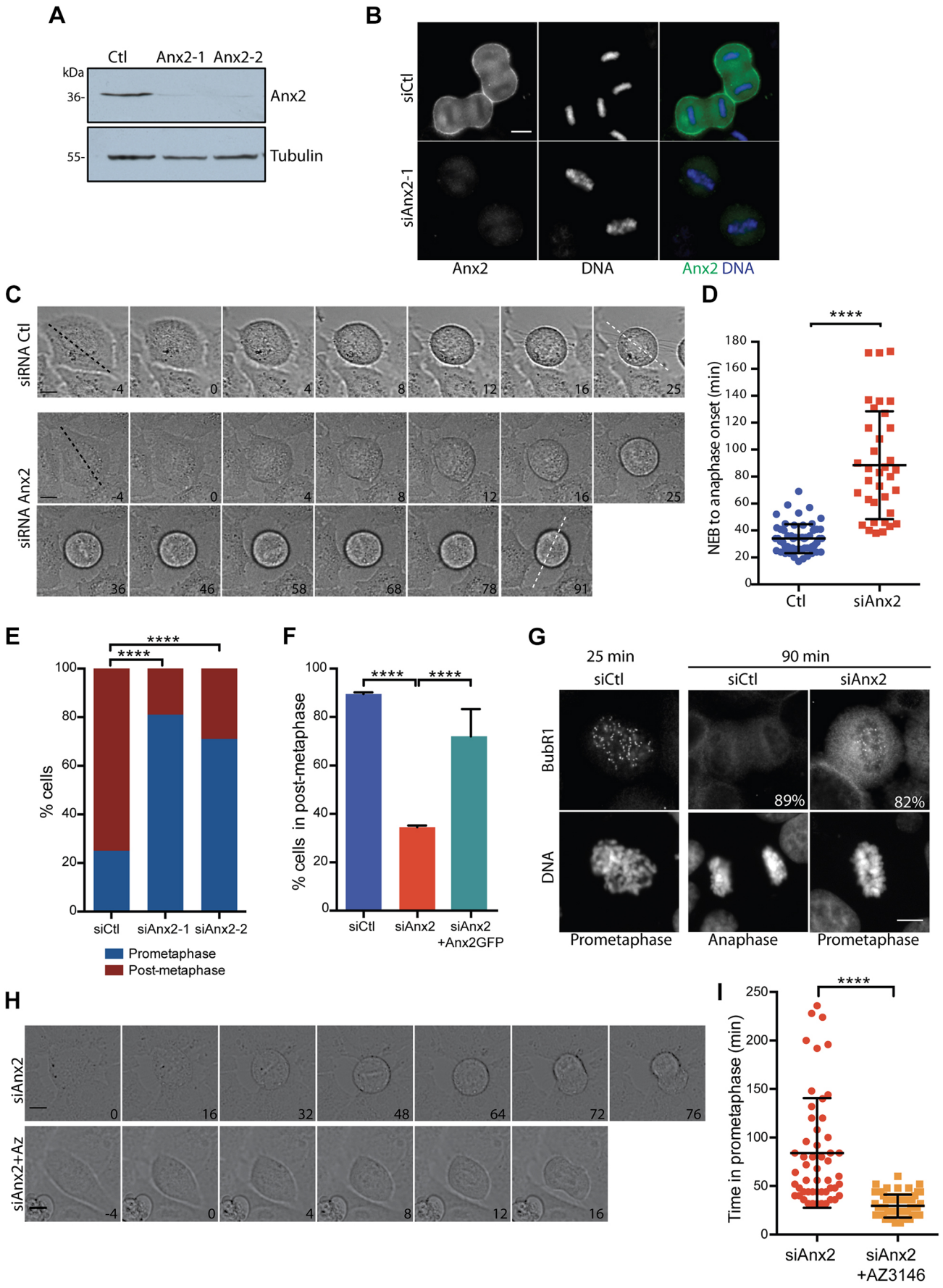

Fig. 1. See next page for legend.

Journal of Cell Science

Journal of Cell Science (2022) 135, jcs259344. doi:10.1242/jcs.259344

Fig. 1. Silencing of Anx2 results in prolonged prometaphase. (A) Western blot of HeLa cells transfected with control siRNA (Ctl) or two independent Anx2 siRNAs (Anx2-1, Anx2-2). (B) Immunostaining of the control (siCtl) and Anx2 siRNA-treated cells (siAnx2-1) 60 min after G2/M synchronization release. Anx2 is in green and DNA in blue. Scale bar: 10 µm. Images shown in A,B are representative of three independent experiments. (C) Time-lapse phase-contrast images of asynchronously dividing cells treated with control or Anx2 siRNAs, from prophase to anaphase. Scale bars: 10 µm. *t0*, nuclear envelope breakdown (NEB). The black dotted lines indicate the Feret's diameters, which predict the axis of division (*t*=−4), and the white ones the actual axis of division (*t*=25 and 91). Time: min. (D) Graph showing the time elapsed from the NEB to onset of anaphase in control (*n*=56) and Anx2-silenced cells (*n*=35). ****P<0.0001 (Mann–Whitney *U* test). (E,F) Quantification of metaphase-to-anaphase progression in control cells and cells treated with Anx2 siRNAs alone or with siRNAs together with siRNA-resistant Anx2–GFP at 90 (E) or 70 min (F) after G2/M (*n*>80 cells). ****P<0.0001 (Fisher's exact test). (G) BubR1 staining in control and Anx2 siRNA-treated cells, 25 min (prometaphase) or 90 min (anaphase or arrested metaphase) after G2/M synchronization release. The percentage of cells with the illustrated phenotype is indicated on the panels (*n*>50). Scale bar: 5 µm. (H) Live-cell phase-contrast images of asynchronous Anx2 siRNA-treated HeLa cells in presence of DMSO (siAnx2) or 2 µM of the Mps1 inhibitor AZ3146 (siAnx2+AZ) during early cell division. Scale bars: 10 µm, time: min. (I) Quantification of the time spent in prometaphase for control (Anx2 siRNA) and Mps1 inhibitor-treated cells (Anx2 siRNA+AZ3146) (*n*=58). ****P<0.0001 (Mann–Whitney *U*-test). All graphs show mean±s.d. from three independent experiments.

anaphase 34±10.7 min (mean±s.d.) after nuclear envelope breakdown (NEB), cells treated with Anx2 siRNAs (siAnx2) displayed a mean time of 83±40.1 min (Fig. 1C,D). Furthermore, 46% of the treated cells failed to enter anaphase within 180 min. Both Anx2 siRNAs resulted in similar phenotypes, with 81% (siRNA-1) and 71% (siRNA-2) of the cells blocked in prometaphase 90 min after G2/M release, as compared to 25% in the control (Fig. 1E). Co-transfection with a siRNA-resistant Anx2–GFP construct rescued the siRNA-induced mitotic delay, with 71.5±8.5% of the cells progressing into anaphase as compared to 34.5±0.5% when the cells were treated with Anx2 siRNA alone (*t*=70 min) (Fig. 1F). To address whether the delay in the metaphase-anaphase transition observed in Anx2-depleted cells was due to the activation of the mitotic checkpoint (spindle assembly checkpoint; SAC), we looked for the presence of the active SAC marker BuBR1 on the kinetochore of mitotic cells. Immunofluorescence analysis showed that 90 min after G2/M release it was detectable at the kinetochore of 82% the Anx2-depleted prometaphase cells (Fig. 1G). Furthermore, treatment of Anx2 siRNA-treated cells with AZ3146, an inhibitor of the Mps1 kinase (encoded by *TTK*) required for the assembly of the SAC (Hewitt et al., 2010), abolished the delay induced by Anx2 depletion (Fig. 1H,I). These results indicate Anx2 depletion induces a SAC-dependent anaphase onset delay.

Anx2 regulates spindle orientation

In early prometaphase, cell retraction fibers dictates the orientation of the mitotic spindle (Kunda and Baum, 2009). As a consequence, rounding control cells rapidly orient their metaphasic plate perpendicular to the adhesion plane to divide along the cell length (Feret's diameter) (Toyoshima and Nishida, 2007). By contrast, metaphase plate rotation was observed in Anx2-depleted cells (Fig. 1C), prompting us to investigate spindle orientation. While the metaphase plate displayed an *x*-*y* oscillation within 20.7±11° (mean±s.d.) along the final axis of division in the control cells, Anx2-depleted cells showed a large amplitude one direction rotation (78.4±48°) (Fig. 2A,B). In addition, in the *x*-*z* axis, the metaphase plate of the control cells remained, as expected, mostly perpendicular to the adhesion plane, whereas we observed rotations along the *z*-axis in Anx2-depleted cells (Fig. 2A, dotted line). We thus measured the spindle angles relative to the adhesion plane at fixed times (Fig. 2C). In control cells, the distribution of *x*-*z* spindle angles was indeed constrained at an average of 7.5±1.7°. In contrast, the spindle angle measurements in Anx2-depleted cells exhibited a wider distribution (Fig. 2D). Indeed, 86% of control cells had a spindle angle less than 15°, compared to 55.5% of the Anx2-depleted cells. Expression of siRNA-resistant Anx2 restored the correct spindle angle in 76% of cells (Fig. 2E). Our results thus indicate that Anx2 is required for mitotic spindle orientation.

Anx2 is a cortical mitotic protein

We next examined the localization of Anx2 in prometaphase using a HeLa cell line that stably expresses Anx2–GFP. At mitotic entry, Anx2 was enriched at the retracting cortex, adjacent to the retraction fibers, and became concentrated at the cortex facing the spindle poles in late prometaphase and metaphase (Fig. 2F–H). A similar localization was observed for the endogenous protein in mitotic HeLa cells (Fig. 2L) and in MDCK cells (Fig. S3A).

This restricted cortical localization of Anx2 suggests that adhesion cues may influence Anx2 localization. Fibronectin-coated micropatterns that constrain cell adhesion have been used to demonstrate the influence of retraction fibers on the cortical segregation of mitotic spindle orientation cues and in the regulation of the axis of division (Théry et al., 2005, 2007). We therefore examined Anx2 localization in mitotic cells plated on L-shaped micropatterns. As expected for a protein whose localization is influenced by adhesion cues, Anx2 was enriched at the cortex facing the adhesive side of prometaphase cells (Fig. 2I,J). This enrichment was apparent as early as prophase, before the NEB and mitotic spindle formation (Fig. S1A, *t*=0, 3 min). As the mitotic spindle has been shown to influence the localization of the spindle-anchoring complex (Kiyomitsu and Cheeseman, 2012; Gallini et al., 2016), we examined the potential contribution of the mitotic spindle on Anx2 distribution. Upon disruption of the mitotic spindle formation by nocodazole treatment, the cortical localization of Anx2 was not abolished (Fig. S1C), indicating that recruitment of Anx2 at the mitotic cortex does not require the mitotic spindle.

When plated on fibronectin-coated L-shaped micropatterns, the constrained adhesion drives the orientation of the division axis and cells divide along the hypotenuse of the L shape (Théry et al., 2005). Indeed, 92% of the control mitotic spindles were positioned with an angle of 126±30.8° (mean±s.d.; Fig. 2K). In contrast, when Anx2 was depleted, a wide range of angles was observed. To exclude that the spindle orientation defect observed is due to a loss of adhesion upon Anx2 depletion, we controlled that Anx2-depleted cells retained their ability to adhere and spread on fibronectin (Fig. S1D). Taken together, these results show that Anx2 is required for adhesion-driven regulation of mitotic spindle orientation.

Anx2 controls Ahnak cortical localization during mitosis

To explore the molecular functions of Anx2, we looked for candidate proteins that interact with Anx2 at the mitotic cortex. In interphase epithelial cells, the $(Anx2–S100A10)_2$ tetramer forms a complex with Ahnak at the cortex, where it has been suggested to structure cortical domains (Benaud et al., 2004; De Seranno et al., 2006; Grieve et al., 2012). To investigate whether Ahnak binds to the Anx2 tetramer in the context of mitotic spindle orientation, we performed co-immunoprecipitation experiments in Anx2–GFP-expressing metaphase HeLa cells. Endogenous S100A10 and Ahnak both co-immunoprecipitated with Anx2–GFP, but neither

Journal of Cell Science (2022) 135, jcs259344. doi:10.1242/jcs.259344

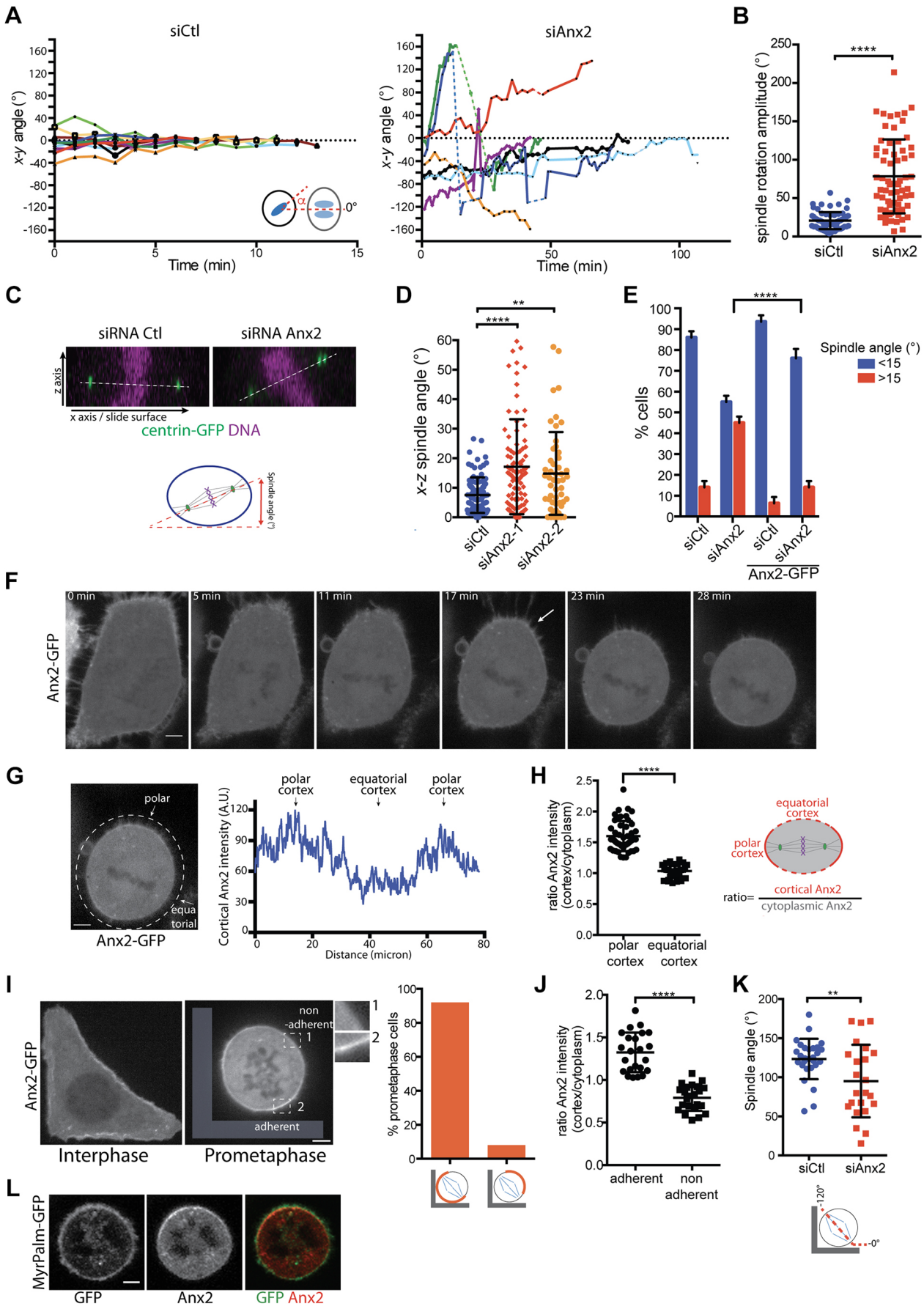

Fig. 2. See next page for legend.

Journal of Cell Science

Journal of Cell Science (2022) 135, jcs259344. doi:10.1242/jcs.259344

Fig. 2. Anx2 localizes at the prometaphase cell cortex and is required for spindle orientation. (A) Plot over time of the metaphase plate oscillation in the *x*-*y* plane from late prometaphase to anaphase onset in asynchronized control HeLa cells (siCtl, left) and cells depleted for Anx2 (siAnx2, right). The angles were measured relative to the metaphase plate position at anaphase onset as depicted in the diagram. Dotted line indicates when the metaphase plate is no longer in the plane due to *x*-*z* rotation (siAnx2 panel). (B) Plot of the maximal spindle rotation amplitude in control cells (n=68) and Anx2-depleted cells (n=66). ****P<0.0001 (unpaired two-tailed Student's t-test). (C) Top, confocal *x*-*z* projection images of contol and Anx2 siRNA-treated metaphase GFP–centrin cells stained for centrin (anti-GFP) and DNA (To-Pro-3). Bottom, schematic diagram of the spindle angle measurement. (D) Distribution of mitotic spindle angles relative to the adhesion plane in control cells (n=98) and in cells treated with Anx2 siRNA-1 (n=94) or Anx2 siRNA-2 (n=51). **P=0.0018; ****P<0.0001 (Mann–Whitney U test). (E) Percentage of cells with correct spindle orientation (<15°) in control cells (n=88), cells treated with Anx2 siRNA (n=105), control siRNA+Anx2–GFP (n=51), and Anx2 siRNA+Anx2–GFP (n=43). ****P<0.0001 (Fisher's exact test). In D and E, spindle angles were measured as depicted in C in synchronized late prometaphase cells (40 min post-mitotic entry). (F) Spinning-disk time-lapse projections of Anx2–GFP cells throughout prophase and prometaphase. Arrow indicates Anx2 enrichment at the cortex adjacent to adhesion fibers. Images shown in F are representative of three independent experiments. (G) Spatial distribution of Anx2 along the cortex in late prometaphase. Right, relative fluorescent intensity profile of Anx2–GFP measured at the cortex (dotted line, left). (H) Quantification of Anx2–GFP cortex/cytoplasm intensity ratio at the polar and the equatorial cortex (n=48), as depicted on the diagram. ****P<0.0001 (Mann–Whitney U test). (I) Left, spinning disk image of live Anx2–GFP cells plated on L-shaped micropatterns in interphase and prometaphase. Two insets highlight localizations. Right, percentage of prometaphase cells displaying the Anx2–GFP cortical localization depicted in orange on the schematic diagram below (n=24). (J) Quantification of the data illustrated in I (prometaphase), presented as the ratio of Anx2–GFP intensity (cortex/cytoplasm) on the cortex facing the adherent side and the non-adherent side (n=24). ****P<0.0001 (unpaired two-tailed Student's t-test). (K) Distribution of the mitotic spindle angle in control and Anx2-depleted cells plated on L-shaped micropatterns (n≥23 cells). A schematic of the spindle orientation is shown below. **P=0.0051 (Mann–Whitney U test). (L) Confocal immunofluorescence image of endogenous Anx2 in HeLa MyrPalm-GFP prometaphase cells. TCA-fixed cells were stained with anti-GFP (green) to visualize membrane and anti-Anx2 (red). Images shown in L are representative of three independent experiments. All graphs show means±s.d. from three independent experiments. Scale bars: 5 µm.

did with GFP alone (Fig. 3A). Conversely, Anx2 was also present in Ahnak immunoprecipitates from metaphase cell extracts (Fig. 3B). Previous crystallography analysis has indicated that the Anx2–S100A10-binding domain on Ahnak spans both the Anx2 and the S100A10 proteins (Ozorowski et al., 2013). We therefore speculated that impeding the formation of the Anx2–S100A10 tetramer should also prevent formation of the Ahnak–Anx2 complex. As predicted, Ahnak did not co-immunoprecipitate with an Anx2 mutant that contained two amino acid substitutions (I7L9/EE) that impede S100A10 binding (Thiel et al., 1992) (Fig. 3J).

To investigate Ahnak localization during mitosis, we generated a CRISPR/Cas9 HeLa cell line to tag endogenous Ahnak with GFP. Live time-lapse analysis showed a localization of Ahnak at the cortex (Fig. 3C). In prometaphase, Ahnak was enriched at the retracting cortex, and asymmetrically accumulated at the cortex facing the spindle poles in metaphase (Fig. 3C). As the cell progressed to anaphase, Ahnak was then symmetrically distributed on the cortex facing both spindle poles. The polarized distribution of Ahnak at the cortex facing spindle poles at prometaphase was confirmed by immunostaining of endogenous Ahnak in HeLa cells (Fig. 3D,F). In addition, visualization of retractation fibers by ezrin, radixin and moesin (ERM) staining (Tsukita and Yonemura, 1999) in early prometaphase highlighted the accumulation of Ahnak at the cortex facing the adhesion points (Fig. S1B). Furthermore, immunostaining indicated that both Anx2 and Ahnak colocalize at the cortex in metaphase (Fig. 3E). As seen for Anx2, the localization of Ahnak during prometaphase pointed to the influence of adhesion. Strikingly, the cortical localization of Ahnak was also not disrupted by impeding mitotic spindle formation (Fig. S1C). In prometaphase cells plated on L-shape micropatterns, Ahnak was enriched in the cortex facing the adhesive side (Fig. 3G,H), and this localization was reduced by 72% upon Anx2 depletion [77.9±8% versus 21.9±6.4% (mean±s.d.) enrichment at the cortex facing the adhesive side versus the cortex facing the non-adhesive side in control and Anx2 depleted cells, respectively] (Fig. 3I). A similar reduction in cortical Ahnak intensity was observed in adherent cells expressing the I7L8/EE-Anx2 mutant (Fig. 3K,L). Conversely, depletion of Ahnak also resulted in 19% decrease in Anx2 intensity at the cortex, suggesting that both proteins tend to stabilize each other at the cortex (Fig. S2). Altogether, these results indicate that the Anx2 tetramer interacts with Ahnak at the cortex during prometaphase, and that it regulates the distribution of Ahnak in the cortex.

Loss of cortical Ahnak alters mitotic spindle orientation

We next examined whether alteration in Ahnak levels and localization mimics the effect of Anx2 depletion on mitotic progression and spindle orientation. The siRNA depletion of Ahnak was confirmed by western blotting (Fig. 4A). This resulted in a delay in mitotic progression, with only 34.5% of the depleted cells reaching anaphase 60 min after the G2/M release compared to 77% of the control cells (Fig. 4B). Metaphase measurements of the spindle angle relative to the adhesive surface indicated a significantly wider distribution of spindle angles in both Ahnak-depleted cells and in cells expressing the Ahnak-binding deficient I7L8/EE-Anx2 mutant (Fig. 4C).

We further used time-lapse analyses of GFP-labeled mitotic spindles for live imaging of mitotic spindle orientation in prometaphase cells (Fig. 4D). Only modest *x*-*y* oscillations were observed in the control cells. In contrast, cells depleted for Ahnak or Anx2, or with altered Ahnak localization due to the expression of the I7L8/EE-Anx2 mutant, displayed both mitotic spindle bending and spindle rotation in the *x*-*y* as well as in the *z*-axis. In addition, we observed a 38.5% and 58% decrease in relative astral microtubules intensity in Anx2 and Ahnak depleted cells compared to control cells (Fig. 3E,F). To confirm the key role of Ahnak on mitotic spindle orientation, we also examined the consequences of Ahnak downregulation in MDCK cells (Fig. S3). In MDCK cells, astral microtubules are anchored to the lateral membrane domain to position the spindle parallel to the substrate. *Z*-axial analysis of Anx2 and Ahnak localization indicates that they are enriched at the lateral cortex facing the spindle pole (Fig. S3A). Similar to our observations in HeLa cells, downregulation of Ahnak by siRNA (Fig. S3B) resulted in an increase in spindle bending observed and in a wider range of metaphase spindle angle distribution relative to the adhesion plane (Fig. S3C,D). Overall, our results strongly suggest that Anx2 promotes the cortical recruitment of Ahnak in order to control spindle orientation.

Ahnak influences the distribution of the dynein–dynactin complex in the cortex

The mitotic spindle is anchored to the cell cortex through the interaction of cortical NuMA with the dynein–dynactin microtubule motor (Kotak and Gönczy, 2013). The restricted distribution at the cortex of both proteins is necessary for the robust orientation of the mitotic spindle (Grava et al., 2006; Kiyomitsu and Cheeseman, 2012). The observation that in the absence of cortical Ahnak

Journal of Cell Science (2022) 135, jcs259344. doi:10.1242/jcs.259344

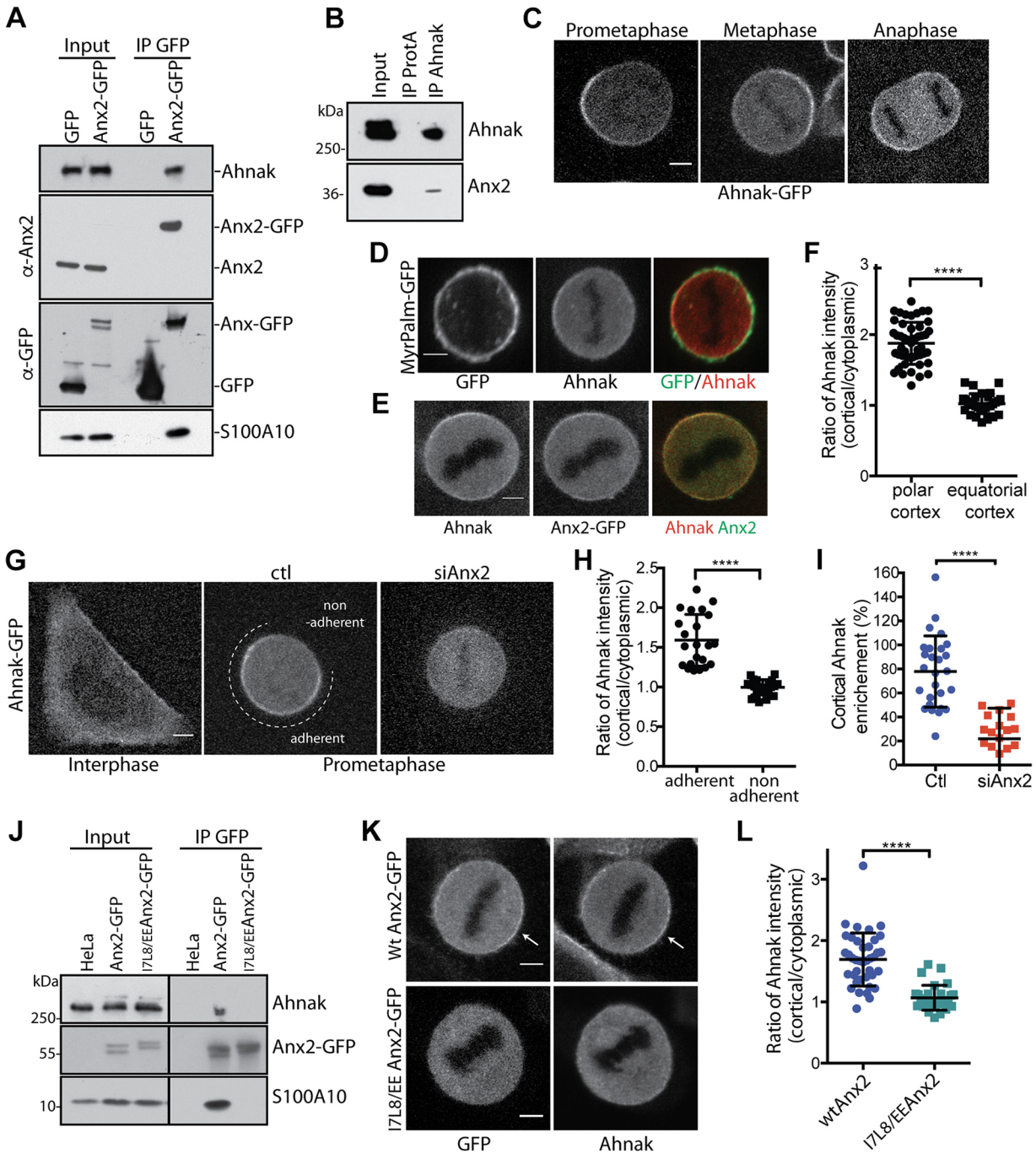

Fig. 3. Anx2 binds to Ahnak and controls its cortical localization in metaphase. (A) Western blots of GFP immunoprecipitates (IP) from metaphase cell extracts of HeLa cells expressing GFP alone or Anx2–GFP. Blots were probed for Ahnak, Anx2, GFP and S100A10. Input lanes show 1% of the extract used. (B) Western blot of control and Ahnak immunoprecipitates from metaphase cells extracts probed for Ahnak and Anx2. (C) Live spinning-disk images of Ahnak–GFP mitotic cells. (D) Immunofluorescence image of endogenous Ahnak staining (red) in TCA-fixed metaphasic HeLa MyrPalm–GFP cells (anti-GFP, green). (E) Confocal image of endogenous Ahnak (red) and Anx2 (anti-GFP, green) staining in TCA fixed metaphase Anx2-GFP cells. Images shown in A–E are representative of three independent experiments. (F) Quantification of Ahnak cortex/cytoplasm intensity ratio at the polar and the equatorial cortex (n=50), as depicted on the diagram in Fig. 2H. ****P<0.0001 (unpaired two-tailed Student's t-test). (G) Spinning-disk images of live Ahnak–GFP localization in interphase and prometaphase cells treated with control or Anx2 siRNAs, and plated on L-shaped micropatterns. (H) Quantification of cortical Ahnak intensity (cortex/cytoplasm) at the cortex facing the adherent side and the cortex facing the non-adherent side in Ahnak–GFP cells (G, prometaphase Ctl). n=22, ****P<0.0001 (Mann–Whitney U-test). (I) Quantification of the relative percentage of Ahnak enrichment on the cortex facing the adherent side (dotted line in G) [100×(I adherent−I nonadherent)/(I nonadherent) where I is intensity] in control cells (n=27) and Anx2-depleted cells (n=24). ****P<0.0001 (Mann–Whitney U-test). (J) GFP immunoprecipitates from metaphase cell extracts of control cells and of cells expressing either Anx2–GFP or I7L8/EE-Anx2–GFP were analyzed by western blotting for the presence of the corresponding GFP-tagged proteins (anti-GFP), Ahnak and S100A10. Input lanes show 1% of the extract used. Images shown in J are representative of three independent experiments. (K) Immunostaining of Ahnak in mitotic cells expressing Anx2–GFP or I7L8/EE-Anx2-GFP using anti-GFP and anti-Ahnak antibodies. Arrows indicate the cortex facing spindle poles. (L) Quantification of cortical Ahnak enrichment (cortical/cytoplasmic intensity) in control metaphase cells (wtAnx2) (n=40) and in cells expressing I7L8/EE-Anx2 mutant (n=30). ****P<0.0001 (Mann–Whitney U-test). All graphs show mean±s.d. from three independent experiments. Scale bars: 5 µm.

Journal of Cell Science (2022) 135, jcs259344. doi:10.1242/jcs.259344

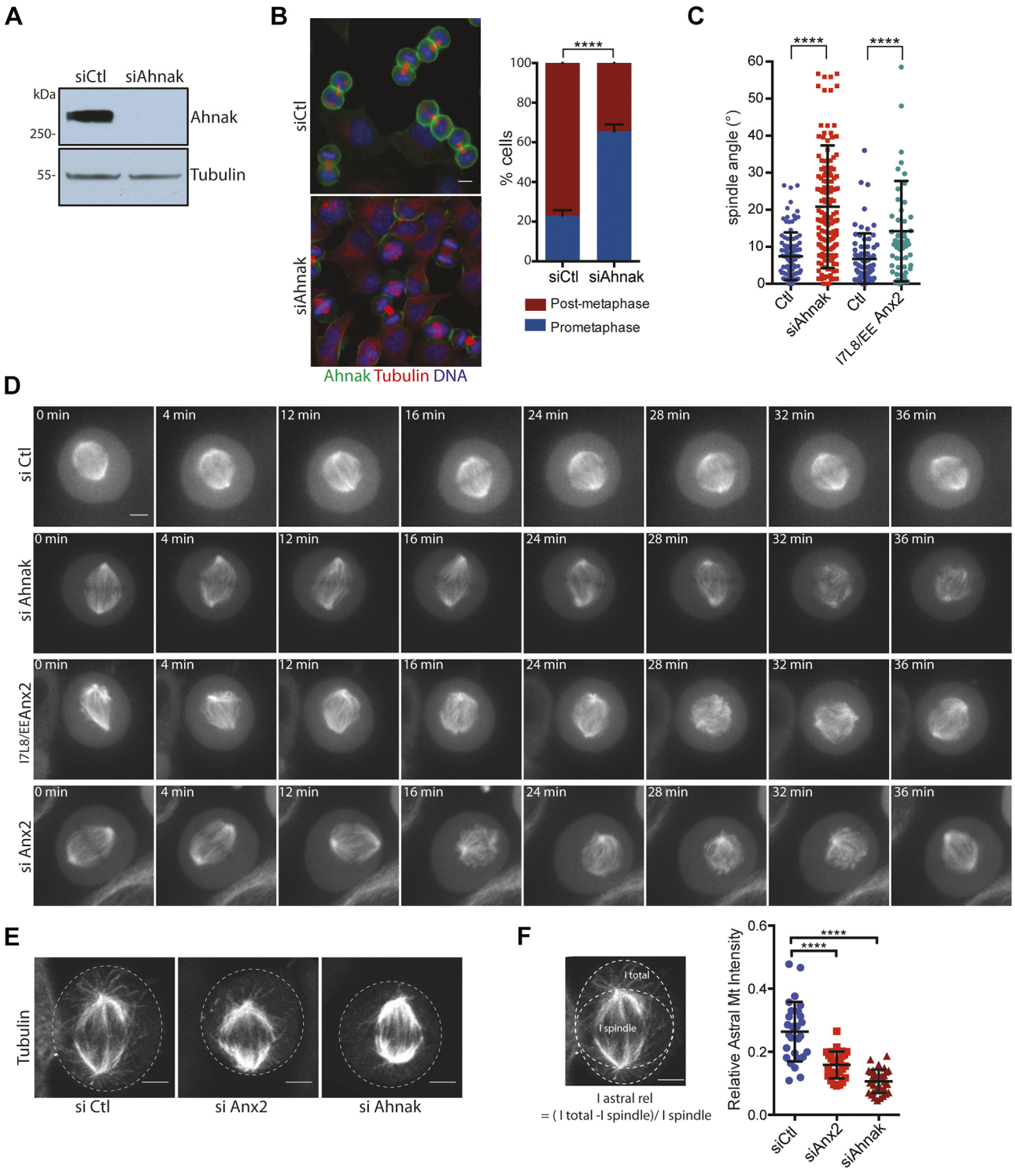

Fig. 4. Ahnak-silencing induces prometaphase delays and mitotic spindle misorientation. (A) Western blot of HeLa cells treated with control or Ahnak siRNA. (B) Left, Ahnak (green), tubulin (red) and DNA (blue) staining in control cells and cells silenced for Ahnak, 60 min after G2/M synchronization release. Scale bar: 10 µm. Right, quantification of mitotic stage repartition (n>94 cells). ****P<0.0001 (Fisher's exact test). (C) Distribution of spindle angles relative to adhesion planes in control centrin–GFP cells (n=101) and in cells either depleted of Ahnak (n=158) or expressing the I7L8/EE-Anx2 mutant (n=71). ****P<0.0001 (Mann–Whitney U test). Quantification performed as in Fig. 2D. (D) Z-stack projection images of mitotic tubulin–GFP control cells and cells expressing Ahnak siRNA, Anx2 siRNA or the I7L8/EE-Anx2 mutant, illustrating spindle distortion and rotation. Acquisition performed in the presence of MG132. (E) α-tubulin staining of control, Anx2 siRNA- or Ahnak siRNA-treated metaphase cells. (F) Quantification of relative astral microtubule intensity for control (n=28), Anx2 siRNA (n=28) and Ahnak siRNA (n=33)-treated cells, calculated as depicted in the left panel. ****P<0.0001 (unpaired two-tailed Student's t-test). Images shown in A, D and E are representative of three independent experiments. All graphs show means±s.d. from three independent experiments. Scale bars: 5 µm.

Journal of Cell Science (2022) 135, jcs259344. doi:10.1242/jcs.259344

(Ahnak siRNAs and Anx2 mutants) there is defective orientation in the spindle, led us to investigate the influence of Ahnak on the spindle-anchoring machinery. We first immunoprecipitated Ahnak from metaphase HeLa cell extracts. Western blots indicated that the dynein–dynactin complex was present in these immunoprecipitates (Fig. 5A). We thus investigated the consequences of Ahnak depletion on cortical dynein localization. Live confocal imaging of HeLa cells expressing GFP-tagged dynein heavy chains (DYNC1H1; DynHC–GFP) revealed that, unlike in control metaphase cells, where dynein was clearly present on centrosomes and on the cortex facing the spindle poles, dynein intensity was strongly reduced at the cortex proximal to the poles following Ahnak depletion (Fig. 5B).

As previously reported (Kiyomitsu and Cheeseman, 2012), dynamic observation of dynein in control cells showed that it oscillated from one spindle pole and its facing cortex to the other throughout prometaphase. This dynein movement was tightly associated with metaphase plate oscillation (Fig. 5C; Movie 1). Both Ahnak and Anx2 depletion altered the lateral oscillation of cortical dynein (Fig. 5C; Movies 2 and 3). The dynein enrichment on the cortex facing the spindle poles was detected in 92.7% of the control cells, but only in 15.3% and 20.2% of the cells depleted for Ahnak or Anx2, respectively (Fig. 5D). Dynein targeting to the kinetochore could still be observed under either Ahnak- or Anx2-knockdown conditions (Fig. 5C, kymographs; Movies 1–3). Immunostaining of the $p150^{Glued}$ subunit (also known as DCTN1) of the dynactin complex in metaphase cells also showed an absence of dynactin enrichment at the cortex facing the poles in 80.5% of the Ahnak-depleted cells (Fig. 5F,H) and in 82.1% of the cells expressing the I7L8/EE-Anx2 mutant (Fig. 5G,H). It is interesting to note that, together with the disorganization of cortical dynein, we also observed reduced metaphase plate oscillations and slower rates of chromosome alignment in metaphase plates (Fig. 5C). Indeed, whereas 90% of the control cells had aligned their chromosomes into a metaphase plate 40 min following mitotic entry, only 10.1% and 19.5% of the cells depleted for Ahnak and Anx2, respectively, had aligned all their chromosomes into a metaphase plate at that time (Fig. 5E).

We next set out to examine whether the crescent-shaped enrichment of NuMA at the mitotic cell cortex was also altered in absence of cortical Ahnak and Anx2. Whereas 87% of the control cells exhibited a polarized cortical localization of NuMA, this was observed in only 25% of the Anx2 siRNA-treated cells, 22.2% of the Ahnak siRNA-treated cells and 3% of the cells expressing the I7L8/EE-Anx2 mutant (Fig. 5I,J). Furthermore, NuMA localization was restored in 75.5% of the cells when an siRNA-resistant Anx2 was expressed (Fig. 5J).

Taken altogether, our results suggest that alterations in cortical Ahnak disrupt the cortical distribution of the NuMA–dynein spindle anchoring complex.

DISCUSSION

At mitotic onset, the cell cortex reorganizes to sustain cell division (di Pietro et al., 2016). This reorganization is characterized by the recruitment and the spatial restriction at the cortex of the highly conserved spindle-anchoring components that bind astral microtubules and contribute to the orientation of the mitotic spindle (Kiyomitsu and Cheeseman, 2012). We have identified here Anx2–Ahnak as crucial cortical players implicated in mitotic spindle orientation. Indeed, absence or altered localization of Ahnak–Anx2 results in a misorientation of the mitotic spindle that displays a slow drift through time, which is indicative of a weakened anchorage of the spindle to the cell cortex.

In addition to spindle misorientation, cells with altered Anx2 and Ahnak displayed several mitotic defects. The spindles were frequently distorted and bended, and chromosome alignment to the metaphase plates was delayed. These defects were accompanied by impaired mitotic progression caused by the activation of the spindle assembly checkpoint. Absence of Anx2 and Ahnak localization on the mitotic spindle and the kinetochore argue against a direct role in mitotic spindle assembly. Although the exact mechanism remains to be defined, similar SAC-dependent metaphase-anaphase transition delay and chromosomes congression defects have been described upon alteration of mitotic cortical organizers (Kschonsak and Hoffmann, 2018; Zhu et al., 2013). Interestingly, Ahnak- and Anx2-depleted cells display reduced numbers of astral microtubules. It is therefore possible that the mitotic defects observed in these cells are caused to some extent by this loss of astral microtubules. Interestingly, reduction in astral microtubules associated with spindle orientation defects have also been reported when the cortical actin-associated protein MISP is depleted (Zhu et al., 2013). Most strikingly, the presence of Anx2 and Ahnak at the cortex is required for the restricted cortical localization of the NuMA–dynein spindle-anchoring complex. Furthermore, Ahnak and Anx2 are present in a protein complex associated with cortical dynein and dynactin. However, whether there is direct or an indirect interaction through the assembly of a larger macromolecular cortical complex remains to be determined. The mitotic spindle assembly defects observed in our study could therefore also be the consequence of the alteration in the cortical localization NuMA–dynein, thereby affecting the spindle architecture and leading to spindle distortion, as observed in dynein heavy chain-knockout cells (Hueschen et al., 2017). The reduced lateral spindle oscillation observed in Ahnak- and Anx2-depleted cells can also derive from the disruption of the constrained cortical localization of the NuMA–dynein anchoring complex (Kiyomitsu and Cheeseman, 2012; Kotak et al., 2012).

Our localization experiments reveal that Anx2 and Ahnak localize together at the cortex above retraction fibers during early prometaphase and the following mitotic steps. Their localization appears to be partly co-dependent; Anx2 is required to recruit Ahnak to the cortex, but only a moderate decrease in cortical Anx2 is observed in the absence of Ahnak. Moreover, our data also reveal that Anx2 and Ahnak act in a complex at the cortex to regulate the anchoring of the mitotic spindle in response to adhesion cue. In patterned cells, Anx2 and Ahnak are enriched at the cortex facing the adhesive side as early as prophase entry, and their downregulation impairs adhesion-directed spindle orientation. Preventing mitotic spindle formation does not reduce their presence at the cortex, indicating that signal arising from the mitotic spindle is not the major driver for their cortical localization. Interestingly, the increase in cortical Anx2 observed in presence of nocodazole suggests that microtubules instead play a role in their dynamics after their cortical recruitment. We cannot exclude that, as described for the components of the anchoring complex (Gallini et al., 2016; Kiyomitsu and Cheeseman, 2012), the mitotic spindle contributes in constraining Anx2–Ahnak cortical localization.

Spindle orientation and anchoring complex localization are highly dependent on the actin cortex. Cortical actin depolymerization, as well as depletion of actin organizers, results in loss of spindle orientation regulation (Théry et al., 2005; Toyoshima and Nishida, 2007; Zhu et al., 2013). Concomitantly, the integrity of the actin cortex is required for proper cortical NuMA and dynein localization (Kschonsak and Hoffmann, 2018; Machicoane et al., 2014; Théry et al., 2005; Zhu et al., 2013). In several cellular contexts, Anx2 has been associated with dynamic actin at the site of membrane

Journal of Cell Science (2022) 135, jcs259344. doi:10.1242/jcs.259344

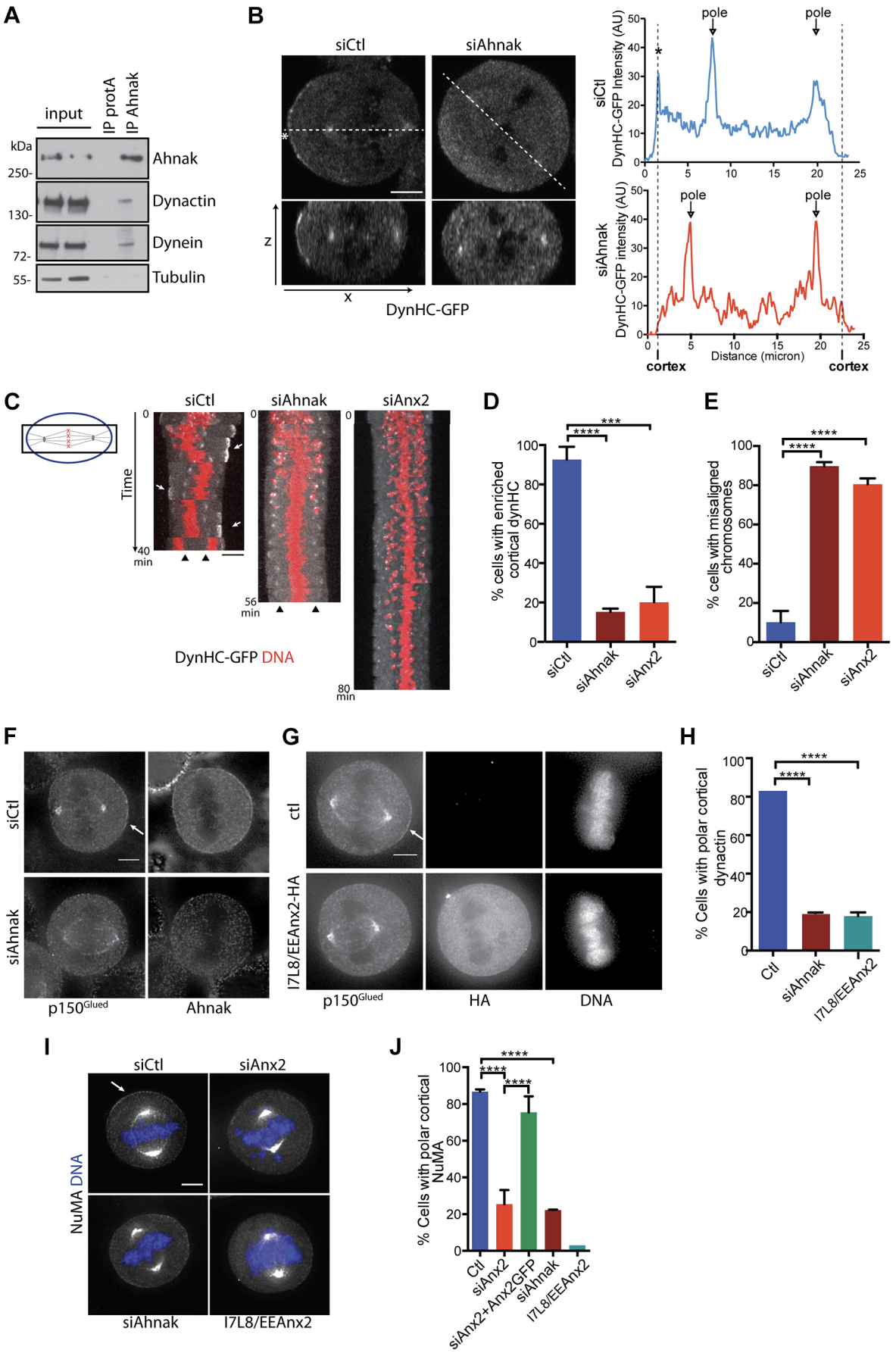

Fig. 5. See next page for legend.

Journal of Cell Science

Journal of Cell Science (2022) 135, jcs259344. doi:10.1242/jcs.259344

Fig. 5. Ahnak interacts with dynein-dynactin complex and is required for NuMA–dynein proper cortical localization during prometaphase. (A) Ahnak and control immunoprecipitates from metaphase HeLa cell extracts were subjected to western blot staining for Ahnak, the p150^{Glued} dynactin subunit, the dynein intermediate chain subunit and tubulin. Input lanes show 1% of the extract used. (B) Left, live fluorescence image of mitotic cells expressing the dynein heavy chain tagged GFP (DynHC–GFP). Single *x*-*y* confocal planes (top panel) and *z*-*x* projections (bottom panel) of cells transfected with control or Ahnak siRNA are shown. Right, intensity profiles of DynHC–GFP along the dashed line. The asterisk points to the dynein cortical peak present in control but not Ahnak-depleted cells. (C) Kymographs generated from spinning-disk time-lapse acquisitions (4-min intervals) of mitotic DynHC–GFP (white) cells expressing H2B–mCherry (red). Dynein localization in control cells and in cells depleted for either Ahnak or Anx2 is shown from prophase to anaphase. Metaphase delays are visible in Ahnak and Anx2 siRNA. Arrows point to the cortical oscillation of dynein in control cells, and arrowheads indicate its centrosomal localization. Full sequences are available in Movies 1–3. Images shown in A–C are representative of three independent experiments. (D) Percentage of metaphase cells displaying enriched cortical dynein at the spindle poles in controls or in cells silenced for Ahnak or Anx2. n>40 cells, ***P<0.0002; ****P<0.0001 (unpaired two-tailed Student's t-test). (E) Quantification of chromosome alignment 40 min after mitosis entry in control cells (n=65) and cells depleted for Ahnak (n=72) or Anx2 (n=83). ****P<0.0001 (Fisher's exact test). (F) Staining of the p150^{Glued} subunit of dynactin and Ahnak in control cells or cells silenced for Ahnak. Arrow points to cortical dynactin toward the spindle poles. (G) Staining of p150^{Glued} in controls or cells expressing I7L8/EE-Anx2 mutant (anti-HA). (H) Graph showing the percentage of cells (n>50) that display polar cortical dynactin localization. ****P<0.0001 (unpaired two-tailed Student's t-test). (I) NuMA staining in prometaphase control cells, cells depleted for Anx2, Ahnak or expressing the I7L8/EE Anx2 mutant. Arrow points to NuMA at the cortex facing the spindle poles (siCtl). (J) Quantification of the percentage of cells displaying NuMA at the cortex facing the spindle pole in Ctl (n=56), Anx2 (n=55) and Ahnak (n=50) siRNA-treated cells or in cells expressing the I7L8/EE-Anx2 mutant (n=35), and Anx2–GFP cells treated with Anx2 siRNA (n=50). ****P<0.0001 (Fisher's exact test). All graphs show means±s.d. from three independent experiments. Scale bars: 5 µm.

remodeling and has been shown to orchestrate the establishment of defined cortical domains (Grieve et al., 2012). Our results indicate that the Anx2 complex also contributes to the mitotic cortical organization in early mitosis. At this stage, we cannot exclude that loss of Anx2 impact mitotic actin cortex remodeling and cortical F-actin organization, thereby triggering spindle orientation defects (Kunda and Baum, 2009). Alternatively, Anx2 might also be involved in defining cortical domains and contributes in restricting the anchoring complex localization within the cortex.

Interestingly, Anx2 displays high affinity for PIP-containing membranes (Hayes et al., 2004; Rescher et al., 2004) and it recruits effector to these sites (Grieve et al., 2012). During mitosis, the lipid composition of the mitotic plasma membrane has been shown to directly influence the establishment of proper spindle orientation. In metaphase, PIPs are enriched in the membrane domains facing the spindle poles and they are required for cortical dynein–dynactin recruitment (Toyoshima et al., 2007), as well as driving and constraining the cortical distribution of NuMA (Kotak et al., 2014). We show that both Anx2 and Ahnak are enriched at the retracting cortex in prometaphase and at the cortex facing the spindle pole in metaphase, a localization that parallels the cortical localization of the spindle-anchoring protein dynein (Movie 1) (Kiyomitsu and Cheeseman, 2012). Furthermore, the restricted cortical localization of Ahnak is hindered by both Anx2 depletion and the expression of an Anx2 mutant that does not bind Ahnak. Anx2 might thus target Ahnak to the PIP-enriched plasma membrane domains and ensure Ahnak initial stabilization at the cortex. By organizing cortical platforms, they might contribute to stabilization and restraining NuMA–dynein localization, favoring the lateral concentration of NuMA–dynein clusters required to generate pulling forces on the spindle (Okumura et al., 2018).

We propose that the Anx2–Ahnak pathway collaborates with other systems to structure cortical hallmarks and sustain spindle orientation. The core components of the cortical force complex are highly conserved throughout evolution (Morin and Bellaïche, 2011). However, Ahnak has appeared later in evolution, with the vertebrates. It is thus tempting to speculate that Ahnak participates in cortical organization strategies that vertebrates may have evolved. Taken together, our study has highlighted a new element in the integrative system that transduce external cue information to the mitotic spindle.

MATERIALS AND METHODS

Cell culture and synchronization

HeLa Kyoto cells (Benaud et al., 2015) and MDCK cells (Benaud et al., 2004) were grown in Dulbecco's modified Eagle's medium Glutamax supplemented with 10% fetal calf serum (Gibco), 100 U/ml penicillin and 100 µg/ml streptomycin (complete medium). For synchronization experiments, cells were treated for 16 h with 5 µM RO-3306 (Merck), washed in complete medium and released for the indicated times. For synchronization in metaphase, cells synchronized at the G2/M transition were released for 40 min and collected by mitotic shake off. For Mps1 inhibition, cells were images in presence of 2 µM AZ3146 (Calbiochem). To visualize mitotic spindle orientation live, HeLa cells expressing tubulin–GFP were released for 40 min to reach metaphase and then imaged in presence of 5 µM MG132 (Calbiochem) to prevent anaphase onset. For micropattern experiments, cells were plated on fibronectin coated L-shaped micropattern chips (CYTOO, Grenoble) according to the manufacturer's instructions. For adhesion experiment, cells depleted for Anx2 or Ahnak by means of siRNA were trypsinized and allowed to adhere and spread on fibronectin (Gibco)-coated coverslips (4 µg/cm^2) overnight.

Expression constructs and stable cell lines

Plasmids Anx2GPF, I7L8/EEAnx2GFP, I7L8/EEAnx2HA have been previously described (Benaud et al., 2015). The HeLa Ahnak–GFP cell line was generated by CRISPR/Cas9. Single-guide (sg)RNA was designed against the C-terminal Ahnak-coding sequence, upstream of the stop codon, using http://chopchop.cbu.uib.no. The guide sequence was cloned into PX458mCherry (Zhang lab, Broad Institute, USA) encoding for sgRNA scaffold and spCas9. To generate the donor plasmid, 350-nucleotide sequences on each side of the Ahnak stop codon were amplified by PCR from HeLa cell genomic DNA (Nucleospin Tissue, Machery Nagel). Both homology domains were then cloned on each side of the GFP sequence, containing a flexible linker on its N-terminal end, in the PUC19 plasmid using In-Fusion HD cloning kit (Takara Bio). sgRNA/Cas9 plasmid and donor plasmid were co-transfected in HeLa cells using jetPRIME transfection reagents (Polyplus transfection). Cells stably expressing GFP were sorted by FACS, and resulting clones analyzed by western blotting for the expression of Ahnak–GFP, using anti-GFP and anti-Ahnak antibodies. HeLa cells expressing dynein heavy chain tagged with GFP (DynHC–GFP) were obtained from MitoCheck, and stably transfected with H2B–mCherry (Addgene 20972). HeLa cells stably expressing Anx2–GFP (Benaud et al., 2015), tubulin–GFP and centrin–GFP (Pirani et al., 2020), and MyrPalm–GFP (Benaud et al., 2015) have been previously described.

siRNA and plasmids transfection

20 nM of control, Ahnak siRNA, Anx2 siRNA 1 (Benaud et al., 2004) or Anx2 siRNA 2 (Zobiack et al., 2003) were transfected using Lipofectamine RNAiMax reagent (Life Technology) for 36 h before mitotic analysis (immunofluorescence and video microscopy). For transient rescue experiments, 20 nM siRNA and plasmid for Anx2 or I7L8/EEAnx2 were co-transfected with jetPRIME transfection reagents (Polyplus transfection).

Antibodies, immunoblotting and immunofluorescence

The following antibodies were used: α-tubulin (clone YL1/2, cat. no. MAB1864, Millipore; 1:1000), anti-BUBR1 (clone 9, cat. no. 15846199,

BD bioscience; 1:500), anti-GFP (clone 7.1 and 13.1, cat. no. 11814460001, Roche; 1:1000), anti-annexin II (cat. no. 610068, BD Transduction Laboratories; 1:1000), anti-annexin II light chain (cat. no. 610070, BD Transduction Laboratories; 1:1000), anti-HA.11 (clone 16B12, cat. no. MMS-101P, Covence; 1:1000), anti-p150^{Glued} (cat. no. 610473, BD Transduction Laboratories; 1:1000), anti-dynein IC (clone 74.1, cat. no. MAB1618, Millipore, 1:1000), anti-Ahnak (KIS and CQL antibodies, a gift from Jacques Baudier, U873 CEA-Grenoble, France; Benaud et al., 2004; Gentil et al., 2003), anti-NuMA (NB500-174, Novus Biologicals, 1:1000). DNA was stained with Hoechst 33342 or To-Pro-3 iodide (Invitrogen).

For immunofluorescence staining, cells were grown on glass coverslips and fixed with either methanol or trichloroacetic acid (TCA). For TCA fixation, cells were incubated with 10% TCA for 10 min at room temperature before permeabilization with 0.1% Triton X-100 for 5 min. TCA fixation was used for Ahnak, Anx2, p150^{Glued} and NuMA staining in prometaphase cells. For astral microtubules quantifications, cells were plated on fibronectin (4 µg/cm^2)-coated coverslips and fixed in 4% paraformaldehyde (PFA) in cytoskeletal buffer (10 mM MES pH 6.1, 138 mM KCl, 3 mM MgCl, 2 mM EGTA) with 0.004% sucrose for 10 min before permeabilization with 0.1% Triton X-100 for 3 min. Antibody staining was then performed as described previously (Benaud et al., 2004). BubR1 staining was performed as previously described (Pirani et al., 2020).

For immunoprecipitation, cells collected in metaphase were lysed in lysis buffer [10 mM Tris-HCl pH 7.5, 150 mM NaCl, 0.5 mM EDTA, 0.5% NP-40, protease inhibitors (cOmplete Tablets EASYpack, Roche)]. For GFP immunoprecipitation, cells lysates were incubated for 1 h at 4°C with GFP-Trap Magentic Agarose beads (Chromotek). For Ahnak immunoprecipitation, CQL antibody was pre-coupled to Dynabeads Protein A (Invitrogen) according to manufacturer's instruction and incubated with cell lysate for 1 h at 4°C.

Measure of spindle angle

Centrin–GFP HeLa cells were synchronized at the G2/M transition and realized for 40 min to reach late prometaphase. Methanol-fixed cells were stained for GFP and To-Pro-3 iodine to visualize centrosomes and DNA, respectively. Cells showing metaphase plates were imaged by confocal *z* sectioning (0.6 µm). Spindle angles were measured with the Image J software on *xz* projections through the spindle poles. The angle tool was used to measure the angle formed by lines going through the centrosomes and the substrate.

Quantification of cortical intensity

Quantification of cortical Ahnak and Anx2 were measured in prometaphase cells 40 min after synchronized G2/M release. *Z*-sectioning spinning disk images for live imaging or confocal images for fixed samples were acquired. Cortical intensity was measured with the line tool from Max projection of three *z*-sections through the middle of the cell, as depicted in the figures. The ratio of cortical to cytoplasmic intensity is presented.

Live-cell imaging and microscopy

For live imaging, cells were plated in Lab-Tek I chambered cover-glasses (Nunc) or on micropattern chips and imaged in Leibovitz L15 medium without Phenol Red (Gibco) at 37°C (fluorescence imaging) or complete medium (bright-field imaging).

Bright-field images of dividing cells were acquired every 4 min with a 25×/0.75PL Fluotar objective on a DMRIBE inverted microscope (Leica) equipped with CO_2-infused heated incubator chamber and a CoolSNAP ES BW camera (Roper Scientific). Time-lapse fluorescence images were acquired on a spinning disk microscope using a Plan Apo 60×/1.4 NA objective on Eclipse Ti-E microscope (Nikon) equipped with a spinning disk (CSU-X1; Yokogawa), a thermostatic chamber (Life Imaging Service), Z Piezo stage (Marzhauser), and a charge-coupled device camera (CoolSNAP HQ2; Roper Scientific). Time-lapse images were acquired every 4 min using the Metamorph Software (Universal imaging). Ahnak–GFP images were acquired with a 60×/1.4 NA objective on an inverted LeicaDMi8 microscope driven by Inscoper Imaging Suite equipped with a spinning disk CSU-X1 (Yokogawa), a thermostatic chamber and an EmCCD camera. Live DynHC–GFP images were acquired with a 63×/1.4 NA objective on inverted Axio Observer 7 microscope equipped with confocal scan head LSM 880 (Zeiss) and temperature control.

Immunofluorescence images of fixed samples were acquired with either a 40×/1.0 NA objective on DMRXA2 epifluorescence microscope (Leica), a 60×/1.42 NA objective on a LED illuminated Deltavision equipped with a CoolSnapHQ Princeton BW camera, or with a 63×/1.4 NA objective on a SP5 confocal microscope (Leica).

Images were processed and quantified using Fiji software (http://fiji.sc/). Movies were constructed from image stacks saved in AVI 5 fps with Fiji software.

Statistical analysis

Data analyses and statistical tests were performed using the Prism7 software (Graphpad) on data derived from at least three independent experiments. The Mann–Whitney and unpaired two-tailed Student's *t*-tests were used to compare the means of independent samples with non-normal distribution or normal distribution, respectively. The Fisher's exact test was used to assess differences between proportions.

Acknowledgements

We thank S. Dutertre and X. Pinson at the Microscopy Rennes Imaging Center (MRic, BIOSIT, Biogenouest) for assistance. MRic is member of the national infrastructure France-BioImaging supported by the French National Research Agency (ANR-10-INBS-04).

Competing interests

The authors declare no competing or financial interests.

Author contributions

Conceptualization: C.B.; Methodology: A.P., E.G., R.G.; Investigation: A.P., C.B.; Writing - original draft: C.B.; Writing - review & editing: E.G., R.G.; Supervision: R.G., C.B.; Funding acquisition: R.G., C.B.

Funding

E.G. is supported by la Foundation pour la Recherche Medicale (DEQ20170336742). This work was supported by La Ligue Régionale Contre le Cancer (Grand Ouest-Bretagne).

Peer review history

The peer review history is available online at https://journals.biologists.com/jcs/article-lookup/doi/10.1242/jcs.259344.

References

Benaud, C. and Prigent, C. (2016). Annexin A2: a new player in mitosis. *Cell Cycle* **15**, 9-10. doi:10.1080/15384101.2015.1115643

Benaud, C., Gentil, B. J., Assard, N., Court, M., Garin, J., Delphin, C. and Baudier, J. (2004). AHNAK interaction with the annexin 2/S100A10 complex regulates cell membrane cytoarchitecture. *J. Cell Biol.* **164**, 133-144. doi:10.1083/jcb.200307098

Benaud, C., Le Dez, G., Mironov, S., Galli, F., Reboutier, D. and Prigent, C. (2015). Annexin A2 is required for the early steps of cytokinesis. *EMBO Rep.* **16**, 481-489. doi:10.15252/embr.201440015

De Seranno, S., Benaud, C., Assard, N., Khediri, S., Gerke, V., Baudier, J. and Delphin, C. (2006). Identification of an AHNAK binding motif specific for the Annexin2/S100A10 tetramer. *J. Biol. Chem.* **281**, 35030-35038. doi:10.1074/jbc.M606545200

di Pietro, F., Echard, A. and Morin, X. (2016). Regulation of mitotic spindle orientation: an integrated view. *EMBO Rep.* **17**, 1106-1130. doi:10.15252/embr.201642292

Gallini, S., Carminati, M., De Mattia, F., Pirovano, L., Martini, E., Oldani, A., Asteriti, I. A., Guarguaglini, G. and Mapelli, M. (2016). NuMA phosphorylation by Aurora-A orchestrates spindle orientation. *Curr. Biol.* **26**, 458-469. doi:10.1016/j.cub.2015.12.051

Gentil, B. J., Delphin, C., Benaud, C. and Baudier, J. (2003). Expression of the giant protein AHNAK (desmoyokin) in muscle and lining epithelial cells. *J. Histochem. Cytochem.* **51**, 339-348. doi:10.1177/002215540305100309

Grava, S., Schaerer, F., Faty, M., Philippsen, P. and Barral, Y. (2006). Asymmetric recruitment of dynein to spindle poles and microtubules promotes proper spindle orientation in yeast. *Dev. Cell* **10**, 425-439. doi:10.1016/j.devcel.2006.02.018

Grieve, A. G., Moss, S. E. and Hayes, M. J. (2012). Annexin A2 at the interface of actin and membrane dynamics: a focus on its roles in endocytosis and cell polarization. *Int. J. Cell Biol.* **2012**, 852430. doi:10.1155/2012/852430

Hayes, M. J., Merrifield, C. J., Shao, D., Ayala-Sanmartin, J., Schorey, C. D., Levine, T. P., Proust, J., Curran, J., Bailly, M. and Moss, S. E. (2004). Annexin 2 binding to phosphatidylinositol 4,5-bisphosphate on endocytic vesicles is regulated by the stress response pathway. *J. Biol. Chem.* **279**, 14157-14164. doi:10.1074/jbc.M313025200

Hewitt, L., Tighe, A., Santaguida, S., White, A. M., Jones, C. D., Musacchio, A., Green, S. and Taylor, S. S. (2010). Sustained Mps1 activity is required in mitosis to recruit O-Mad2 to the Mad1-C-Mad2 core complex. *J. Cell Biol.* **190**, 25-34. doi:10.1083/jcb.201002133

Hueschen, C. L., Kenny, S. J., Xu, K. and Dumont, S. (2017). NuMA recruits dynein activity to microtubule minus-ends at mitosis. *eLife* **6**, e29328. doi:10.7554/eLife.29328

Kiyomitsu, T. and Cheeseman, I. M. (2012). Chromosome- and spindle-pole-derived signals generate an intrinsic code for spindle position and orientation. *Nat. Cell Biol.* **14**, 311-317. doi:10.1038/ncb2440

Kotak, S. and Gönczy, P. (2013). Mechanisms of spindle positioning: cortical force generators in the limelight. *Curr. Opin. Cell Biol.* **25**, 741-748. doi:10.1016/j.ceb.2013.07.008

Kotak, S., Busso, C. and Gönczy, P. (2012). Cortical dynein is critical for proper spindle positioning in human cells. *J. Cell Biol.* **199**, 97-110. doi:10.1083/jcb.201203166

Kotak, S., Busso, C. and Gönczy, P. (2014). NuMA interacts with phosphoinositides and links the mitotic spindle with the plasma membrane. *EMBO J.* **33**, 1815-1830. doi:10.15252/embj.201488147

Kschonsak, Y. T. and Hoffmann, I. (2018). Activated ezrin controls MISP levels to ensure correct NuMA polarization and spindle orientation. *J. Cell Sci.* **131**, jcs214544. doi:10.1242/jcs.214544

Kunda, P. and Baum, B. (2009). The actin cytoskeleton in spindle assembly and positioning. *Trends Cell Biol.* **19**, 174-179. doi:10.1016/j.tcb.2009.01.006

Machicoane, M., de Frutos, C. A., Fink, J., Rocancourt, M., Lombardi, Y., Garel, S., Piel, M. and Echard, A. (2014). SLK-dependent activation of ERMs controls LGN-NuMA localization and spindle orientation. *J. Cell Biol.* **205**, 791-799. doi:10.1083/jcb.201401049

Martin-Belmonte, F., Gassama, A., Datta, A., Yu, W., Rescher, U., Gerke, V. and Mostov, K. (2007). PTEN-mediated apical segregation of phosphoinositides controls epithelial morphogenesis through Cdc42. *Cell* **128**, 383-397. doi:10.1016/j.cell.2006.11.051

Morin, X. and Bellaïche, Y. (2011). Mitotic spindle orientation in asymmetric and symmetric cell divisions during animal development. *Dev. Cell* **21**, 102-119. doi:10.1016/j.devcel.2011.06.012

Okumura, M., Natsume, T., Kanemaki, M. T. and Kiyomitsu, T. (2018). Dynein-Dynactin-NuMA clusters generate cortical spindle-pulling forces as a multi-arm ensemble. *eLife* **7**, e36559. doi:10.7554/eLife.36559

Ozorowski, G., Milton, S. and Luecke, H. (2013). Structure of a C-terminal AHNAK peptide in a 1:2:2 complex with S100A10 and an acetylated N-terminal peptide of annexin A2. *Acta Crystallogr. D Biol. Crystallogr.* **69**, 92-104. doi:10.1107/S0907444912043429

Pirani, V., Métivier, M., Gallaud, E., Thomas, A., Ku, S., Chretien, D., Ettari, R., Giet, R., Corsi, L. and Benaud, C. (2020). A novel benzodiazepine derivative that suppresses microtubule dynamics and impairs mitotic progression. *J. Cell Sci.* **133**, jcs239244. doi:10.1242/jcs.239244

Rescher, U., Ruhe, D., Ludwig, C., Zobiack, N. and Gerke, V. (2004). Annexin 2 is a phosphatidylinositol (4,5)-bisphosphate binding protein recruited to actin assembly sites at cellular membranes. *J. Cell Sci.* **117**, 3473-3480. doi:10.1242/jcs.01208

Théry, M., Racine, V., Pépin, A., Piel, M., Chen, Y., Sibarita, J.-B. and Bornens, M. (2005). The extracellular matrix guides the orientation of the cell division axis. *Nat. Cell Biol.* **7**, 947-953. doi:10.1038/ncb1307

Théry, M., Jiménez-Dalmaroni, A., Racine, V., Bornens, M. and Jülicher, F. (2007). Experimental and theoretical study of mitotic spindle orientation. *Nature* **447**, 493-496. doi:10.1038/nature05786

Thiel, C., Osborn, M. and Gerke, V. (1992). The tight association of the tyrosine kinase substrate annexin II with the submembranous cytoskeleton depends on intact p11- and Ca(2+)-binding sites. *J. Cell Sci.* **103**, 733-742. doi:10.1242/jcs.103.3.733

Toyoshima, F. and Nishida, E. (2007). Spindle orientation in animal cell mitosis: roles of integrin in the control of spindle axis. *J. Cell. Physiol.* **213**, 407-411. doi:10.1002/jcp.21227

Toyoshima, F., Matsumura, S., Morimoto, H., Mitsushima, M. and Nishida, E. (2007). PtdIns(3,4,5)P3 regulates spindle orientation in adherent cells. *Dev. Cell* **13**, 796-811. doi:10.1016/j.devcel.2007.10.014

Tsukita, S. and Yonemura, S. (1999). Cortical actin organization: lessons from ERM (ezrin/radixin/moesin) proteins. *J. Biol. Chem.* **274**, 34507-34510. doi:10.1074/jbc.274.49.34507

van Leen, E. V., di Pietro, F. and Bellaïche, Y. (2020). Oriented cell divisions in epithelia: from force generation to force anisotropy by tension, shape and vertices. *Curr. Opin. Cell Biol.* **62**, 9-16. doi:10.1016/j.ceb.2019.07.013

Zhu, M., Settele, F., Kotak, S., Sanchez-Pulido, L., Ehret, L., Ponting, C. P., Gönczy, P. and Hoffmann, I. (2013). MISP is a novel Plk1 substrate required for proper spindle orientation and mitotic progression. *J. Cell Biol.* **200**, 773-787. doi:10.1083/jcb.201207050

Zobiack, N., Rescher, U., Ludwig, C., Zeuschner, D. and Gerke, V. (2003). The annexin 2/S100A10 complex controls the distribution of transferrin receptor-containing recycling endosomes. *Mol. Biol. Cell* **14**, 4896-4908. doi:10.1091/mbc.e03-06-0387